Research Paper

Numerical Study on the Dynamics of a Charged Bubble in the Acoustic Field

Liang LV[(1)], Fei LIU[(2)], Yawei LI[(3)]*

[(1)] *School of Mechano-Electronic Engineering, Suzhou Vocational University*
Suzhou, China

[(2)] *Department of Sports Health and Art Education, Hebei Petroleum University of Technology*
Chengde, China

[(3)] *Department of the Party and the Mass, Hebei Petroleum University of Technology*
Chengde, China

*Corresponding Author e-mail: liyawei_123321@163.com

In this paper, the dynamics of an acoustic bubble with a constant charge in compressible liquid are investigated numerically, which is based on the Gilmore-NASG model to estimate the radial oscillations. The cavitation effects are enhanced due to the presence of the charge on the bubble surface. The obtained results from the present model are compared with that calculated by the previous model within a wide range of parameters (e.g., charge, acoustic pressure amplitude, ultrasound frequency, and liquid temperature). The similar influences of these parameters on bubble collapse intensity can be observed from both models. Since the present model fully considers the compressibility of gas and liquid, it can be applied to a wider parameter range and leads to the larger predicted values. The research in this paper can provide important insights about the effects of charge on bubble dynamics and the acoustic cavitation applications (e.g., sonochemistry, water treatment, and food industry).

Keywords: charged bubble dynamics; acoustic cavitation; bubble collapse intensity; Gilmore-NASG model.

1. Introduction

Cavitation bubbles exist widely in nature, e.g., the snapping shrimp uses cavitation bubbles formed by the rapid closure of its claws to stun its prey; in a fast flowing system, cavitation bubbles are prone to occur if the channel suddenly narrows and then widens. The phenomenon of cavitation in the liquid is concerned because of its damage to hydraulic machinery and ship propellers (SEZEN *et al.*, 2021; WANG *et al.*, 2022). Due to unique physical and chemical phenomena (CLEVE *et al.* 2019; DEHANE *et al.*, 2022; KERBOUA *et al.*, 2021; LV *et al.*, 2019; LV, LIU, 2023; TIAN *et al.*, 2023) (e.g., liquid jet, free radicals formation, radiation pressure, and acoustic microstreaming) caused by the bubble oscillations, cavitation has been contributed to various applications such as water treatment (FERKOU *et al.*, 2015), petroleum hydrocarbons degradation (LEI *et al.*, 2020), nanoparticle synthesis (POKHREL *et al.*, 2016), and so on.

The charges carried on the bubble surface have been reported by many research groups. The zeta potential of the bubble measured experimentally by using the microelectrophoresis technique indicated that the effect of the PH solution on the variation of the bubble zeta potential depended not only on the type of the metal ions but also on the electrolyte concentration (YANG *et al.*, 2001). They also found the charge polarity varied at different solutions (e.g., the bubble was the negative charge in NaCl solutions, while its charge polarity reversed in multivalent metal ions solutions). TAKAHASHI (2005) found that the bubbles were negatively charged under a wide range of the PH condition and positively charged under strongly acidic conditions. In (LEE, CHOI, 2020), the stable light emission of a single bubble sonoluminescence (SBSL bubble)

with charge in water was investigated for the first time. The results revealed that the SBSL bubble was positively charged and suggested that it was necessary for analyses of the SBSL bubble to take the electrical properties into consideration. The behaviour of laser-generated bubbles in an electric field was studied by PHUKAN *et al.* (2023). They found the maximum bubble radius increased with the increase of the electric field intensity. This effect was more pronounced in the presence of an acetone medium and decreased successively in ethanol and water media owing to their varying magnitudes of electrical conductivity. In addition to experimental researches of the bubbles in an electric field, theoretical studies have also made great progress. The volume mode and shape model dynamics were examined in a weakly viscous dielectric fluid under the uniform and the axisymmetric straining electric field (OH *et al.*, 2001). A model was built describing the violent collapse of the bubble in the homogeneous, irrotational, solenoidal, and unsteady electric field (SPELT, MATAR, 2006). The research group optimized the bubble model in the electric field, and further analyzed the bubble dynamics of violent collapse, translation and shape deformations (SHAW *et al.*, 2009).

Nevertheless, there are few studies on the charged bubbles that undergo acoustic cavitation, which has been applied in many fields (e.g., ultrasonic cleaning, drug delivery, and inactivate viruses). Based on the study of the stability of a charged bubble in the dielectric liquid in (GRIGOR'EV, ZHAROV, 2000), the model of a charged bubble excited by ultrasound wave has been deduced by HONGRAY *et al.* (2014; 2015). The study results proved that the effective surface was reduced due to the presence of charge. Compared with the uncharged bubble oscillations under acoustic excitation, the bubble expanded to a larger radius and compressed to a smaller size, which in turn caused the bubble collapse to be stronger. The bifurcation diagrams have also been studied to some extent, with the presence of charge leading to advance bifurcations.

The theoretical and experimental researches have been proved a lot on the charge bubbles in liquid. The theoretical study of bubble dynamics in the acoustic field is mainly based on uncharged bubbles, which will lead a bias in calculation results. The model of charged bubbles was derived from the Keller-Miksis equation (HONGRAY *et al.*, 2014; 2015). When the effect of charge is taken into account, the bubble collapse will be enhanced resulting in the significant increase of the speed of a bubble wall, and the Mach number can easily reach 1, which is the critical value that the Keller-Miksis equation is safely adopted (ZILONOVA *et al.*, 2018). Therefore, it is necessary to establish a model that can be used in large parameter intervals, especially the high pressure amplitude and low frequency excitation. In this paper, based on the Gilmore-NASG model (DENNER *et al.*, 2021), a more applicable dynamic model of charged bubbles is established and compared with the model (HONGRAY *et al.*, 2014; 2015) in detail within a wide range of parameters. Subsequently, the sections of present paper are organized as follows. In Sec. 2, the model of a charged bubble and the numerical method are introduced. In Sec. 3, the calculation results of the present model are quantitatively compared with those of the previous model. In Sec. 4, the main findings of the present paper are summarized.

2. Mathematical model and simulation method

For simplicity, the following assumptions are used in physical models: (1) the bubble is spherically symmetric; (2) the fluid is Newtonian and compressible; (3) the buoyancy force and gravity are neglected; (4) the bubble-bubble interaction is neglected; (5) the thermal conductivity, phase change and mass transport across the bubble-liquid interface are neglected. The radial dynamics of the bubble is governed by the Gilmore equation (DENNER, 2021):

$$\left(1 - \frac{\dot{R}}{c_l}\right)R\ddot{R} + \frac{3}{2}\left(1 - \frac{\dot{R}}{3c_l}\right)\dot{R}^2 = \left(1 + \frac{\dot{R}}{c_l}\right)H$$
$$+ \left(1 - \frac{\dot{R}}{c_l}\right)R\frac{\dot{H}}{c_l}, \quad (1)$$

where R is the instantaneous radius of the bubble, the overdot denotes the time derivative, c_l is the speed of sound in the liquid at the bubble wall, H is the difference between the enthalpy of the liquid at the bubble wall and at infinity. The state of gas and vapor inside the bubble, and the liquid outside the bubble are described by the NASG equation of state, and the expression is (DENNER, 2021):

$$p(v, T) = \frac{(\Gamma - 1)C_V T}{v - b} - B, \quad (2)$$

where p is the pressure, v is the specific volume, T is the temperature, Γ is the polytropic exponent, C_v is the heat capacity at a constant volume, b is the co-volume that represents the volume occupied by the individual molecules, B is a pressure constant that models molecular attraction.

H and c_l are defined as Eqs. (3) and (4), respectively:

$$H = \frac{\Gamma_l}{\Gamma_l - 1}\left(\frac{p_l + B_l}{\rho_l} - \frac{p_\infty + B_l}{\rho_\infty}\right) - b_l\frac{p_l - p_\infty}{\Gamma_l - 1}, \quad (3)$$

$$c_l = \sqrt{\Gamma_l\frac{p_l + B_l}{\rho_l(1 - b_l\rho_l)}}, \quad (4)$$

where Γ_l is the liquid polytropic exponent, p_l is the pressure in the liquid at the bubble wall, B_l is the liquid

pressure constant, p_∞ is the liquid pressure at infinity, ρ_l and ρ_∞ are the densities of liquid at the bubble wall and at infinity, respectively. The expressions of p_l, p_∞, ρ_l, and ρ_∞ are given as Eqs. (5)–(8):

$$p_l = p_g - \frac{2\sigma}{R} - 4\mu\frac{\dot{R}}{R} + \frac{Q^2}{8\pi\varepsilon R^4}, \qquad (5)$$

$$p_\infty = P_{l,0} - P_a \sin(2\pi f t), \qquad (6)$$

$$\rho_l = \frac{K_l(p_l + B_l)^{\frac{1}{\Gamma_l}}}{1 + b_l K_l(p_l + B_l)^{\frac{1}{\Gamma_l}}}, \qquad (7)$$

$$\rho_\infty = \frac{K_l(p_\infty + B_l)^{\frac{1}{\Gamma_l}}}{1 + b_l K_l(p_\infty + B_l)^{\frac{1}{\Gamma_l}}}, \qquad (8)$$

where σ is the surface tension coefficient of the liquid, μ is the viscosity of the liquid, Q is the charge at a bubble surface, ε (i.e., $\varepsilon = 85\varepsilon_0$, ε_0 is the vacuum permittivity) is the liquid permittivity, $P_{l,0}$ is an ambient pressure in the liquid, P_a is the acoustic pressure, f is the ultrasonic frequency, K_l and p_g are the constants representing the liquid reference state and gas pressure inside the bubble, respectively, and expressions are defined as Eqs. (9) and (10):

$$K_l = \frac{\rho_{l,0}}{(\rho_{l,0} + B_l)^{\frac{1}{\Gamma_l}}(1 - b_l\rho_{l,0})}, \qquad (9)$$

$$p_g = (P_{g,0} + B_g)\left[\frac{\rho_{g,0}\left(\frac{R_0}{R}\right)^3(1 - b_g\rho_{g,0})}{\rho_{g,0}\left(1 - b_g\rho_{g,0}\left(\frac{R_0}{R}\right)^3\right)}\right]^{\Gamma_g} - B_g, \qquad (10)$$

where $\rho_{l,0}$ is the predefined reference liquid density, $P_{g,0}$ is the predefined reference gas pressure, $\rho_{g,0}$ is the predefined reference gas density, R_0 is the initial bubble radius, Γ_g is the gas polytropic exponent, B_g is the gas pressure constant.

The temperature of the gas and the liquid at the bubble wall can be calculated by Eq. (11):

$$T = T_0\left(\frac{p + B}{P_0 + B}\right)^{\frac{\Gamma - 1}{\Gamma}}, \qquad (11)$$

where T_0 and P_0 are the reference temperature and pressure, respectively.

Equations (1)–(11) constitute the model of present study, which is called G-M-N-C model. The bubble radial dynamics, sound velocity, liquid density at the bubble wall, gas pressure, gas temperature and liquid temperature are obtained from Eqs. (1), (4), (7), (10), (11), respectively. The fourth term on the right side of Eq. (5) is introduced by considering the charge on the bubble surface. If this term is ignored, the G-M-N-C model is reduced to the model in (DENNER, 2021), which is called the G-M-N model in this paper.

To check the validation of the simulation results, the bubble dynamics obtained by the G-M-N-C model is compared with previous models. A single gas bubble with an initial radius of 3.5 μm oscillating in the water is considered. If not specified, the parameters in present studies are used in Table 1. The models are solved using the method of the Runge-Kutta 4–5 order formula with a variable step length. To obtain the results satisfying the precision requirement, both of the absolute error and relative error are 1×10^{-12}.

Table 1. Parameters keep constant during simulations (DENNER, 2021; HONGRAY *et al.*, 2014; 2015).

Name	Notations	Value	Unit
Gas reference density	$\rho_{g,0}$	1.2	kg/m^3
Liquid reference density	$\rho_{l,0}$	998	kg/m^3
Gas ambient pressure	$P_{g,0}$	1	atm
Liquid ambient pressure	$P_{l,0}$	1	atm
Gas ambient temperature	$T_{g,0}$	300	K
Liquid ambient temperature	$T_{l,0}$	300	K
Gas molecule co-volume	b_g	0	–
Liquid molecule co-volume	b_l	6.7212×10^{-4}	m^3/kg
Gas pressure constant	B_g	0	–
Liquid pressure constant	B_l	6.2178×10^8	Pa
Gas polytropic exponent	Γ_g	1.67	–
Liquid polytropic exponent	Γ_l	1.19	–
Vacuum permittivity	ε_0	8.85×10^{-12}	F/m
Surface tension	σ	7.2×10^{-2}	N/m
Liquid viscosity	μ	1×10^{-3}	Pa·s
Charge on the bubble	Q	0.3	pC

3. Results and discussion

Before showing the dynamics obtained with the G-M-N-C model under various conditions, the other models (i.e., G-M-N in (DENNER, 2021); K-M-C in (HONGRAY *et al.* 2014; 2015)) are adopted to calculate the bubble dynamics under a high amplitude driving acoustic wave in order to conduct the comparative analysis.

Figure 1 shows the predictions obtained by three models, i.e., G-M-N-C, K-M-C, and G-M-N. Most of the variables associated with the bubble are periodic oscillations, except that the sound velocity, the density and temperature of liquid at the bubble wall remain constant calculated by the model of K-M-C. From Fig. 1a, the bubble grows slowly in the initial stage and then rapidly expands to its maximum radius ($R_{\max}$). Correspondingly, the gas temperature and pressure inside the bubble reach the minimum values (Figs. 1c and 1d). At this time, the bubble begins to collapse due to the difference between the inside and outside of the bubble having a maximum value. When the bubble collapse to the minimum radius ($R_{\min}$), according to Figs. 1b–1g, the variable values (i.e., bubble wall velocity, gas temperature and pressure, the temperature, density and sound velocity of liquid on the bubble wall) reach the maximum. After the first collapse, the bubble oscillates slightly several times.
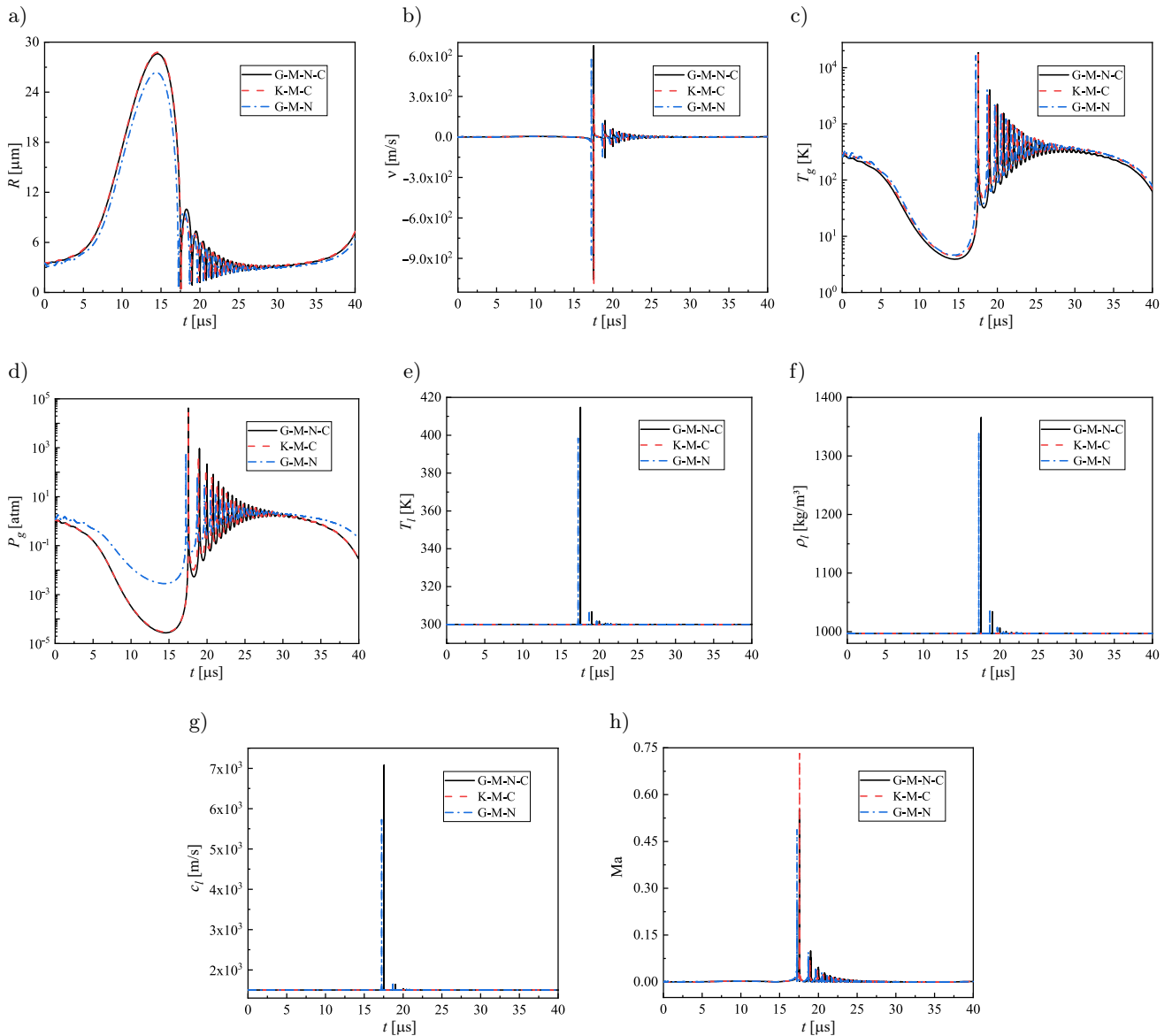
Fig. 1. Time developments of the bubble radius (a), the bubble wall velocity (b), the gas temperature (c) and pressure (d) inside the bubble, the liquid temperature (e), density (f) and sound velocity (g) at the bubble wall, and the Mach number of the bubble wall (h) as retrieved by G-M-N-C model (solid line), K-M-C model (dash line) and G-M-N model (dash dot line). The bubble driven by an ultrasound wave with frequency of 30 kHz and amplitude of 1.35 atm.

Comparing to the predictions obtained by the model of G-M-N, the maximum variable values (i.e., the gas temperature and pressure, bubble wall velocity, liquid temperature, density and sound speed) calculated by the model of G-M-N-C are larger. This owes to the larger absolute value of the maximum pressure difference at the bubble wall in the model of G-M-N-C with the consideration of the charge on the bubble surface. The bubble can absorb more energy during its expansion, reaching a larger size, and a smaller size will be acquired as the bubble collapses.

The dynamics of the charged bubble are commonly predicted by the K-M-C model, which is compared in detail with the G-M-N-C model. As reported in Fig. 1a,

the lower $R_{\min}$ is achieved from the G-M-N-C model (0.42 µm, compared to 0.44 µm for the K-M-C model). Since NASG equation of state is used in G-M-N-C model to describe dynamic features of the gas in the bubble and the liquid at the bubble wall, and the compressibility of the gas in the bubble is fully considered. It is believed that the covolumes of gas molecules should be different with temperature and pressure. The high temperature and pressure environment caused by the bubble collapse results in a smaller covolume of gas molecule, meaning that there is more space for the gas to compress. Therefore, the bubble collapse depth is deeper, and the minimum bubble radius is smaller. Consequently, the bubble can be compressed more,

yielding a much higher gas temperature and pressure inside the bubble, as indicated in Figs. 1c and 1d. This result matches the finding in (Nazari-Mahroo *et al.*, 2018; 2020).

The G-M-N-C model gives the maximum liquid temperature and density at the bubble wall reaching 414.67 K and 1.37×10^3 kg/m^3, respectively, whereas these two variables keep constant in the K-M-C model from Figs. 1e and 1f. The calculations of the Mach number (Ma) for two models are shown in Fig. 1h. It can be seen that the peak Ma calculated by the G-M-N-C model is significantly lower than that predicted by the K-M-C model. The liquid velocity of sound at the bubble wall varies with time in the G-M-N-C model (Fig. 1g), at the instant of the first bubble collapse, the bubble wall velocity and the liquid velocity of sound at the wall are both large (Figs. 1b and 1g), reducing Ma (e.g., Ma = 0.55 from Fig. 1h), and the reliability of the model can be guaranteed. While the liquid velocity of sound at the bubble wall remains constant in the K-M-C model leading to a larger Ma during the first bubble collapse (e.g., Ma = 0.73 from Fig. 1h).

The K-M-C model evolves from the Keller-Miksis equation taking the liquid compressibility into account, which is accurate at Ma < 1 (Zilonova *et al.*, 2018). The G-M-N-C model is derived from the Gilmore equation, which is obtained basing on the variation of liquid sound velocity and integrating the liquid enthalpy directly instead of the liquid pressure. Hence, the bubble dynamics with charge estimated by the G-M-N-C model is accurate for Ma ≤ 2.2 (Zilonova *et al.*, 2018). Figure 2 summarizes the maximum absolute value of Ma in P_a (1.2–3 atm) – f (20–400 kHz) plane for two models. Within the parameters studied, the Ma calculated by the K-M-C model range from 0.02 to 10.60, while the values obtained by the G-M-N-C model are 0.02–4.76. Under a certain parameter, Ma calculated by the latter model is smaller than that from the former model. The example can be seen in Fig. 1h. The positions of the blue curves are Ma = 1 in Fig. 2a and 2.2 in Fig. 2b, respectively, which are the critical values of Ma for the K-M-C model and the G-M-N-C model applied in numerical studies. Under the excitation parameters on the upper left of the curves, the application of the model is safe, while the lower right is not. It can be seen that the G-M-N-C model has a wider application range than the K-M-C model.

In application researches, evaluating the cavitation intensity by calculating the gas temperature or the emitted sound pressure, which is a difficult task, because of the need to obtain the bubble wall velocity, or the acceleration. To this end, it is necessary to measure the cavitation intensity from the radial dynamics of the bubble. There exist several approaches in the literatures, e.g., the compression ratio ($R_{\max}/R_{\min}$) (Hongray *et al.*, 2014; Kalmár *et al.*, 2020; Nazari-
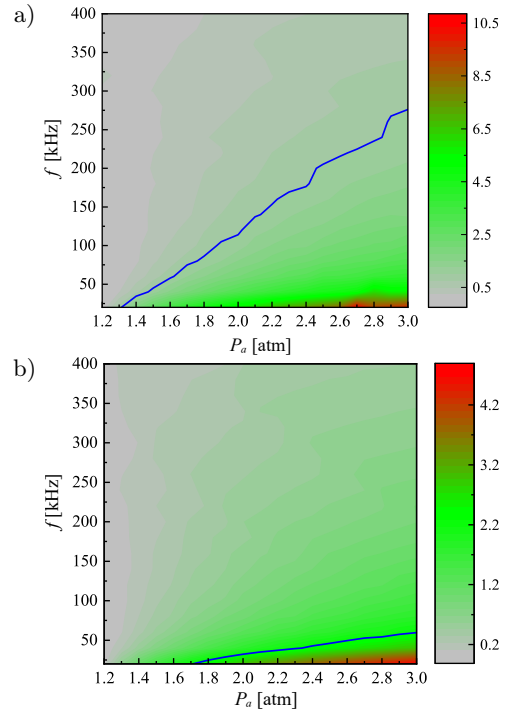

Fig. 2. Maximum absolute value of Mach number of the bubble wall calculated by K-M-C model (a) and G-M-N-C model (b). The numerical results are obtained from more than 200 combinations of ultrasound frequency (20–400 kHz) and acoustic amplitude (1.2–3.0 atm).

Mahroo *et al.*, 2018), the expansion-compression ratio $((R_{\max}-R_0)/(R_0-R_{\min}))$ (Hongray *et al.*, 2015), and the quantity of $\frac{R_{\max}^3}{t_c}$ (Kalmár *et al.*, 2020), where t_c is the bubble collapse time. In the present study, the compression ratio is used to describe the cavitation intensity and is represented by C_s.

The effect of charge Q on the compression ratio C_s is shown in Fig. 3. As can be seen, C_s increases linearly with increasing Q from 0 to 0.6 pC for both models. At the coordinate value of (0.49, 77.36), the two prediction curves intersect. At this time, the minimum bubble radii calculated by two models are similar, and the
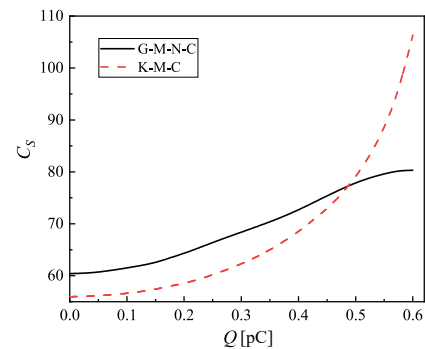

Fig. 3. Compression ratio C_s vs. charge on the bubble, calculated by G-M-N-C model (solid line) and K-M-C model (dash line) for ultrasound frequency of 30 kHz and amplitude of 1.35 atm.

values are about 0.41 µm, which is near the hard-core radius for the bubble with an initial radius of 3.5 µm. Therefore, the variation curves of C_s predicted by two models can only intersect at this point. Also, this result proves the accuracy of the present model. When Q value is away from 0.49 pC, the difference of C_s calculated by two models is increasing. At $Q < 0.49$ pC, the C_s obtained by the G-M-N-C model is larger than that predicted by the K-M-C model. It is worth noting that in the K-M-C model, when Q is greater than 0.53 pC, bubble collapse intensity increases, resulting in Ma > 1 (e.g., at $Q = 0.55$ pC, Ma = 1.03), so that the accuracy of the model is lost. Nevertheless, the range of Q is 0–0.6 pC, and the value of Ma is 0.49–0.61 lying in the application range of the G-M-N-C model.

In order to seek the correlation between the compression ratio C_s and the pressure amplitude P_a, numerical studies have been performed for various P_a (1.2–3.0 atm). The observed results are presented in Fig. 4. With the increase of P_a, C_s calculated by two models increases monotonically. The predicted C_s of the G-M-N-C model is always higher than that of the K-M-C model. The difference of C_s calculated by two models is about 10.02% at P_a from 1.2 to 2.2 atm. When P_a is between 2.2–3.0 atm, the difference increases significantly, and the difference value reaches the maximum at $P_a = 2.4$ atm, which is 51.51%.
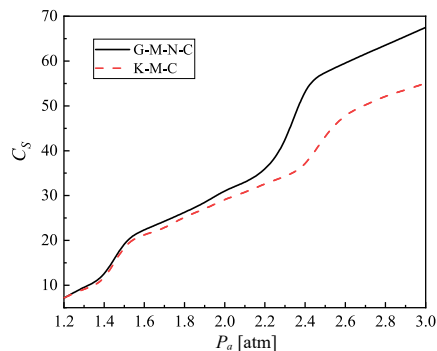

Fig. 4. Compression ratio C_s vs. acoustic amplitude, calculated by G-M-N-C model (solid line) and K-M-C model (dash line) for ultrasound frequency of 30 kHz and charge of 0.3 pC on the bubble.

The effect of ultrasound frequency f on the compression ratio C_s is explored as presented in Fig. 5. It is observed that C_s decreases by increasing f. It is a well-known trend of cavitation bubble dynamics. With the increase of f, there has no enough time to grow for the bubble, resulting in the decrease of C_s. The cavitation intensity is weakened, and the bubble temperature and pressure are reduced. For the two considered models, C_s in the G-M-N-C model is larger than that in the K-M-C model. The difference of C_s calculated by two models reaches the maximum value of 140.51% at the frequency of around 700 kHz.

Other reports in the literatures supported the variation trends of the compression ratio C_s with the pres-
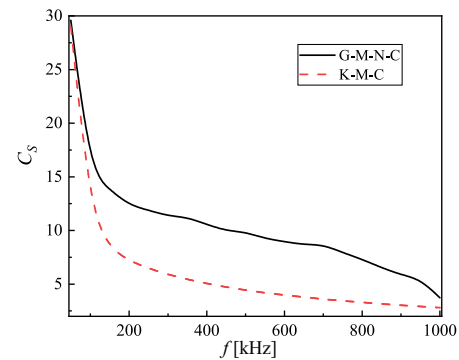

Fig. 5. Compression ratio C_s vs. ultrasound frequency, calculated by G-M-N-C model (solid line) and K-M-C model (dash line) for ultrasound amplitude of 1.35 atm and charge of 0.3 pC on the bubble.

sure amplitude P_a and ultrasound frequency f. FERKOU *et al.* (2015) examined the effect of ultrasound frequency and acoustic intensity on the sonolytic degradation of naphthol blue black in water operating acoustic intensity in the range of 0.44–5.22 W/cm^2 with the frequency in the range of 585–1140 kHz. The observed results indicated that the sonochemical degradation rate increased with increasing acoustic intensity and decreasing the frequency. The similar results were obtained for efficiency of sonochemical degradation Bisphenol A (TORRES *et al.*, 2008), the hydrogen production from a collapsing Ar bubble in water (KERBOUA *et al.*, 2021; DEHANE *et al.*, 2021a) and a collapsing Ar-O$_2$ bubble in methanol (DEHANE *et al.*, 2022).

Figure 6 shows the variation of the compression ratio C_s as a function of liquid temperature T_∞. The cavitation intensity can be enhanced by the increase of T_∞. As can be seen from the figure, the difference (around 10%) between predicted values by two models is not strongly affected by T_∞ from 283 to 333 K. The similar results obtained by Merouani and co-workers (CHADI *et al.*, 2018; DEHANE *et al.*, 2021b; MEROUANI *et al.*, 2014). They found that cavitation intensity and the production ratio of ˙OH generated by a single bub-
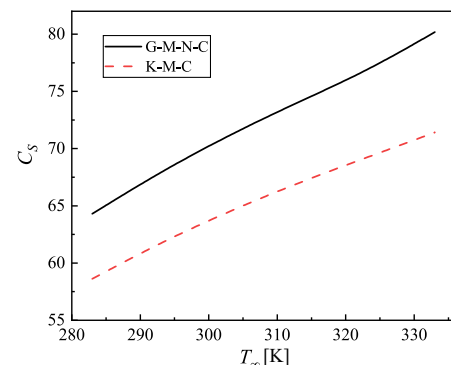

Fig. 6. Compression ratio C_s vs. liquid temperature, calculated by G-M-N-C model (solid line) and K-M-C model (dash line) for ultrasound frequency of 30 kHz, acoustic amplitude of 1.35 atm and charge of 0.3 pC on the bubble.

ble collapse was enhanced with the increase of liquid temperature (CHADI *et al.*, 2018). But the overall production ratio and sonochemical degradation of nonvolatile organic pollutants in aqueous media reached their maximum values at $T_\infty = 50°$. The cavitation effect is mainly affected by the single bubble collapse intensity and the number of bubbles, and the latter decreased with the increase in liquid temperature. DEHANE *et al.* (2021b) found the production of RCS, ·OH, ·H, HCl and HOCl increased proportionally with the increase of liquid temperature (from 10° to 50°) on carbon tetrachloride sono-conversion under acoustic excitation with the intensity of 0.7 W/cm^2 and the ultrasonic frequency of 355 kHz.

Based on the Gilmore-NASG model, the acoustic bubble dynamic model is established in this paper considering the effect of the charge on the bubble surface. The paper analyze the bubble dynamics and cavitation intensity, along with the accuracy of the present model by comparing with the results in the literature. The paper proves the model has a wider range of application parameters. In the future work, present model can be optimized. For example, the effects of bubble-bubble interaction (ZHANG *et al.*, 2016) should be taken into account to investigate the secondary Bjerknes force between two gas bubbles, that coupled with a viscous drag force to analyze the translational motions of the bubbles. The detail results are refered to the works in (WANG *et al.*, 2023). In addition, heat exchange, mass transport and chemical reactions on the dynamics of the bubble with a constant charge are also worth considering (DEHANE *et al.*, 2021a; 2021b; 2022; KERBOUA*et al.*, 2021; LV, LIU, 2023).

4. Conclusion

In the present work, the model for a charged bubble under acoustic excitation is proposed. Compared with the previous model, the proposed model can be applied to a wider parameter range, especially high acoustic amplitudes and low ultrasound frequencies excitation. The bubble collapse intensity calculated by two models is enhanced with increasing charge on the bubble surface, acoustic amplitude and liquid temperature, and the decrease of ultrasound frequency. Except for the charge on the bubble surface, the bubble collapse intensity by the present model is larger under the studied parameter range, mainly because the effect of liquid and gas compressibility is fully considered. When the charge is 0.49 pC, the minimum bubble radius calculated by two models is near the hard-core radius, and the bubble collapse intensity is equal. The differences between predicted values by two models reaches the maximum at $P_a = 2.4$ atm or $f = 700$ kHz, and the liquid temperature has little effect on the difference (around 10%).

References

1. CHADI N.E., MEROUANI S., HAMDAOUI O., BOUHELASSA M. (2018), New aspect of the effect of liquid temperature on sonochemical degradation of nonvolatile organic pollutants in aqueous media, *Separation and Purification Technology*, **200**: 68–74, doi: 10.1016/j.seppur.2018.01.047.

2. CLEVE S., GUÉDRA M., MAUGER C., INSERRA C., BLANC-BENON P. (2019), Microstreaming induced by acoustically trapped, non-spherically oscillating microbubbles, *Journal of Fluid Mechanics*, **875**: 597–621, doi: 10.1017/jfm.2019.511.

3. DENNER F. (2021), The Gilmore-NASG model to predict single-bubble cavitation in compressible liquids, *Ultrasonics Sonochemistry*, **70**: 105307, doi: 10.1016/j.ultsonch.2020.105307.

4. DEHANE A., MEROUANI S., CHIBANI A., HAMDAOUI O., ASHOKKUMAR M. (2022), Influence of processing conditions on hydrogen sonoproduction from methanol sono-conversion: A numerical investigation with a validated model, *Chemical Engineering and Processing – Process Intensification*, **179**: 109080, doi: 10.1016/j.cep.2022.109080.

5. DEHANE A., MEROUANI S., HAMDAOUI O., ALGHYAMAH A. (2021a), A complete analysis of the effects of transfer phenomenons and reaction heats on sonohydrogen production from reacting bubbles: Impact of ambient bubble size, *International Journal of Hydrogen Energy*, **46**(36): 18767–18779, doi: 10.1016/j.ijhydene.2021.03.069.

6. DEHANE A., MEROUANI S., HAMDAOUI O., ABDELLATTIF M.H., JEON B.-H., BENGUERBA Y. (2021b), A full mechanistic and kinetics analysis of carbon tetrachloride (CCl_4) sono-conversion: Liquid temperature effect, *Journal of Environmental Chemical Engineering*, **9**(6): 106555, doi: 10.1016/j.jece.2021.106555.

7. FERKOU H., MEROUANI S., HAMDAOUI O., REZGUI Y., GUEMINI M. (2015), Comprehensive experimental and numerical investigations of the effect of frequency and acoustic intensity on the sonolytic degradation of naphthol blue black in water, *Ultrasonics Sonochemistry*, **26**: 30–39, doi: 10.1016/j.ultsonch.2015.02.004.

8. GRIGOR'EV A.I., ZHAROV A.N. (2000), Stability of the equilibrium states of a charged bubble in a dielectric liquid, *Technical Physics*, **45**(4): 389–395, doi: 10.1134/1.1259640.

9. HONGRAY T., ASHOK B., BALAKRISHNAN J. (2014), Effect of charge on the dynamics of an acoustically forced bubble, *Nonlinearity*, **27**(6): 1157–1179, doi: 10.1088/0951-7715/27/6/1157.

10. HONGRAY T., ASHOK B., BALAKRISHNAN J. (2015), Oscillatory dynamics of a charged microbubble under ultrasound, *Pramana – Journal of Physics*, **84**(4): 517–541, doi: 10.1007/s12043-014-0846-y.

11. KALMÁR C., KLAPCSIK K., HEGEDŰS F. (2020), Relationship between the radial dynamics and the chemical production of a harmonically driven spherical bubble, *Ultrasonics Sonochemistry*, **64**: 104989, doi: 10.1016/j.ultsonch.2020.104989.

12. KERBOUA K., HAMDAOUI O., ISLAM M.H., ALGHYAMAH A., HANSEN H.E., POLLET B.G. (2021), Low carbon ultrasonic production of alternate fuel: Operational and mechanistic concerns of the sonochemical process of hydrogen generation under various scenarios, *International Journal of Hydrogen Energy*, **46**(53): 26770–26787, doi: 10.1016/j.ijhydene.2021.05.191.

13. LV L., LIU F. (2023), Numerical investigation of sonochemical production in a single bubble under dual-frequency acoustic excitation, *Physica Scripta*, **98**(11): 115240, doi: 10.1088/1402-4896/acfeb1.

14. LV L., ZHANG Y.X., ZHANG Y.N., ZHANG Y.N. (2019), Experimental investigations of the particle motions induced by a laser-generated cavitation bubble, *Ultrasonics Sonochemistry*, **56**: 63–73, doi: 10.1016/j.ultsonch.2019.03.019.

15. LEE H.-B., CHOI P.-K. (2020), Electrification of sonoluminescing single bubble, *Journal of Physical Chemistry B*, **124**(15): 3145–3151, doi: 10.1021/acs.jpcb.0c00956.

16. LEI Y.-J., ZHANG J., TIAN Y., YAO J., DUAN Q.-S., ZUO W. (2020), Enhanced degradation of total petroleum hydrocarbons in real soil by dual-frequency ultrasound-activated persulfate, *Science of the Total Environment*, **748**: 141414, doi: 10.1016/j.scitotenv.2020.141414.

17. MEROUANI S., HAMDAOUI O., REZGUI Y., GUEMINI M. (2014), Energy analysis during acoustic bubble oscillations: Relationship between bubble energy and sonochemical parameters, *Ultrasonics*, **54**(1): 227–232, doi: 10.1016/j.ultras.2013.04.014.

18. NAZARI-MAHROO K., PASANDIDEH K., NAVID H.A., SADIGHI-BONABI R. (2018), Influence of liquid compressibility on the dynamics of single bubble sonoluminescence, *Physics Letters A*, **382**(30): 1962–1967, doi: 10.1016/j.physleta.2018.04.058.

19. NAZARI-MAHROO K., PASANDIDEH K., NAVID H.A., SADIGHI-BONABI R. (2020), Influence of liquid density variation on the bubble and gas dynamics of a single acoustic cavitation bubble, *Ultrasonics*, **102**: 106034, doi: 10.1016/j.ultras.2019.106034.

20. OH J.M., KIM P.J., KANG I.S. (2001), Chaotic oscillation of a bubble in a weakly viscous dielectric fluid under electric fields, *Physics of Fluids*, **13**(10): 2820–2830, doi: 10.1063/1.1400135.

21. POKHREL N., VABBINA P.K., PALA N. (2016), Sonochemistry: Science and engineering, *Ultrasonics Sonochemistry*, **29**: 104–128, doi: 10.1016/j.ultsonch.2015.07.023.

22. PHUKAN A., KHARPHANBUH S.M., NATH A. (2023), An empirical experimental investigation on the effect of an external electric field on the behaviour of laser-induced cavitation bubbles, *Physical Chemistry Chemical Physics*, **25**: 2477–2485, doi: 10.1039/d2cp05561a.

23. SEZEN S., UZUN D., TURAN O., ATLAR M. (2021), Influence of roughness on propeller performance with a view to mitigating tip vortex cavitation, *Ocean Engineering*, **239**: 109703, doi: 10.1016/j.oceaneng.2021.109703.

24. SHAW S.J., SPELT P.D.M., MATAR O.K. (2009), Electrically induced bubble deformation, translation and collapse, *Journal of Engineering Mathematics*, **65**(4): 291–310, doi: 10.1007/s10665-009-9314-y.

25. SPELT P.D.M., MATAR O.K. (2006), The collapse of a bubble in an electric field, *Physical Review E*, **74**(4): 046309, doi: 10.1103/PhysRevE.74.046309.

26. TAKAHASHI M. (2005), ζ potential of microbubbles in aqueous solutions: Electrical properties of the gas-water interface, *Journal of Physical Chemistry B*, **109**(46): 21858–21864, doi: 10.1021/jp0445270.

27. TIAN L., ZHANG Y.-X., YIN J.-Y., LV L., ZHANG J.-Y., ZHU J.-J. (2023), Study on the liquid jet and shock wave produced by a near-wall cavitation bubble containing a small amount of non-condensable gas, *International Communications in Heat and Mass Transfer*, **145**(Part A): 106815, doi: 10.1016/j.icheatmasstransfer.2023.106815.

28. TORRES R.A., PÉTRIER P., COMBET E., CARRIER M., PULGARIN C. (2008), Ultrasonic cavitation applied to the treatment of bisphenol A. Effect of sonochemical parameters and analysis of BPA by-products, *Ultrasonics Sonochemistry*, **15**(4): 605–611, doi: 10.1016/j.ultsonch.2007.07.003.

29. WANG C., ZHANG Y., LIU Z., YUAN Z. (2022), Multi-objective optimization of a two-stage liquefied natural gas cryogenic submerged pump-turbine in pump mode to reduce flow loss and cavitation, *Journal of Energy Storage*, **52**(Part C): 105064, doi: 10.1016/j.est.2022.105064.

30. WANG X., NING Z., LV M., WU P., SUN C., LIU Y. (2023), Transition mechanisms of translational motions of bubbles in an ultrasonic field, *Ultrasonics Sonochemistry*, **92**: 106271, doi: 10.1016/j.ultsonch.2022.106271.

31. YANG C., DABROS T., LI D., CZARNECKI J., MASLIYAH J.H. (2001), Measurement of the zeta potential of gas bubbles in aqueous solutions by microelectrophoresis method, *Journal of Colloid and Interface Science*, **243**(1): 128–135, doi: 10.1006/jcis.2001.7842.

32. ZHANG Y., ZHANG Y., LI S. (2016), The secondary Bjerknes force between two under dual-frequency acoustic excitation, *Ultrasonics Sonochemistry*, **29**: 129–145, doi: 10.1016/j.ultsonch.2015.08.022.

33. ZILONOVA E., SOLOVCHUK M., SHEU T.W.H. (2018), Bubble dynamics in viscoelastic soft tissue in high-intensity focal ultrasound thermal therapy, *Ultrasonics Sonochemistry*, **40**(Part A): 900–911, doi: 10.1016/j.ultsonch.2017.08.017.